2005

Spitzer Observations of the Supergiant Shell Region in IC 2574

John M Cannon, *Macalester College*
F. Walter
G. J. Bendo
D. Calzetti
D. A. Dale, et al.

The Astrophysical Journal, 630:L37–L40, 2005 September 1

SPITZER OBSERVATIONS OF THE SUPERGIANT SHELL REGION IN IC 2574

John M. Cannon,[1] Fabian Walter,[1] George J. Bendo,[2] Daniela Calzetti,[3] Daniel A. Dale,[4] Bruce T. Draine,[5] Charles W. Engelbracht,[2] Karl D. Gordon,[2] George Helou,[6] Robert C. Kennicutt, Jr.,[2] Eric J. Murphy,[7] Michele D. Thornley,[8] Lee Armus,[6] David J. Hollenbach,[9] Claus Leitherer,[3] Michael W. Regan,[3] Hélène Roussel,[6] and Kartik Sheth[6]

Received 2005 June 23; accepted 2005 July 28; published 2005 August 16

ABSTRACT

We present spatially resolved *Spitzer Space Telescope* imaging of the supergiant shell region of the M81 group dwarf galaxy IC 2574 obtained as part of the *Spitzer* Infrared Nearby Galaxies Survey. This region harbors one of the best nearby examples of a kinematically distinct H I shell, with an associated remnant stellar cluster; the shell is initiating sequential star formation as it interacts with the surrounding interstellar medium. This region dominates the infrared luminosity of IC 2574 and is spatially resolved in all *Spitzer* imaging bands. We study the differences in dust temperature as a function of local environment and compare local star formation rates as inferred from Hα and total infrared luminosities. We find that the strong Hα sources are associated with regions of warm dust; however, the most luminous infrared and Hα sources are not necessarily cospatial. The coolest dust is found in the regions farthest from the rim of the shell; these regions show the best agreement between star formation rates derived from Hα and from total infrared luminosities (although discrepancies at the factor of 3–4 level still exist). There is considerable variation in the radio–far-infrared correlation in different regions surrounding the shell. The low dust content of the region may influence the scatter seen in these relations; these data demonstrate that the expanding shell is dramatically affecting its surroundings by triggering star formation and altering the dust temperature.

Subject headings: galaxies: dwarf — galaxies: individual (IC 2574) — galaxies: irregular — galaxies: ISM — infrared: galaxies

1. INTRODUCTION

One of the most dramatic effects of vigorous star formation (SF) is the creation of holes and shells in the interstellar medium (ISM). It is commonly proposed that these structures are caused by feedback from massive stars (stellar winds and Type II supernovae [SNe]; e.g., Tenorio-Tagle & Bodenheimer 1988), although alternative scenarios do exist (high-velocity cloud impacts, disk instabilities, turbulence, ram pressure stripping; e.g., Sánchez-Salcedo 2002). Starburst regions and sites of massive cluster formation provide spatially and temporally concentrated feedback that can create the largest of these structures. Holes and shells are therefore a direct, observable signature of the deposit of energy from stars into the ISM.

These structures are found in a great variety of environments, from the Milky Way disk (e.g., McClure-Griffiths et al. 2002) to the ISM of dwarf galaxies (e.g., Walter 1999). After being formed by the combined effects of SNe and stellar winds, the evolution of holes and shells will have a strong environmental dependence; in normal spiral disks, these structures are erased by turbulent motions and rotational shear on timescales of $\sim 10^7$ yr. On the other hand, in dwarf galaxies (typically displaying solid body rotation), rotational shear will not play a major role, and holes and shells may remain coherent until pressure equilibrium is reestablished with the local ISM (e.g., Elmegreen & Hunter 2000). Indeed, studies of active, nearby dwarf galaxies show that these systems are permeated with holes and shells to the H I resolution limit (e.g., the Large Magellanic Cloud, Kim et al. [1999]; the Small Magellanic Cloud, Stanimirovic et al. [1999]; and IC 10, Wilcots & Miller [1998], to name just a few).

IC 2574 is a comparatively large (optical disk ~18 kpc diameter), relatively low metallicity [$12 + \log(\mathrm{O/H}) \simeq 8.15$, or ~30% $Z_\odot$; Miller & Hodge 1996] dwarf galaxy in the M81 group that is undergoing active current SF (Hα-derived SF rate $\mathrm{SFR} \simeq 0.09\ M_\odot\ \mathrm{yr}^{-1}$; Miller & Hodge 1994; Kennicutt 1998). The galaxy hosts a multitude of H I holes and shells (Walter & Brinks 1999), which at the distance of 4.0 Mpc (Karachentsev et al. 2002) provide a unique opportunity to study the SF process and to observe its effects on the surrounding ISM. The most dramatic "supergiant shell" (SGS; Walter et al. 1998; Walter & Brinks 1999) is expanding at ~25 km s^{-1}, has a diameter of ~790 pc, a kinematic age of 15.8 Myr, an H I mass of $\sim 8.2 \times 10^5\ M_\odot$, and requires an energy input of $\sim 5.8 \times 10^{52}$ ergs. As shown in Stewart & Walter (2000), the progenitor stellar cluster is interior to the shell, and the expanding structure is igniting sequential SF on the shell rim.

2. OBSERVATIONS AND DATA REDUCTION

For an overview of the *Spitzer* Infrared Nearby Galaxies Survey (SINGS) observational strategies, see Kennicutt et al.

[1] Max-Planck-Institut für Astronomie, Königstuhl 17, D-69117 Heidelberg, Germany; cannon@mpia.de, walter@mpia.de.
[2] Steward Observatory, University of Arizona, 933 North Cherry Avenue, Tucson, AZ 85721; gbendo@as.arizona.edu, chad@as.arizona.edu, kgordon@as.arizona.edu, robk@as.arizona.edu.
[3] Space Telescope Science Institute, 3700 San Martin Drive, Baltimore, MD 21218; calzetti@stsci.edu, leitherer@stsci.edu, mregan@stsci.edu.
[4] Department of Physics and Astronomy, University of Wyoming, Laramie, WY 82071; ddale@uwyo.edu.
[5] Princeton University Observatory, Peyton Hall, Princeton, NJ 08544; draine@astro.princeton.edu.
[6] California Institute of Technology, MC 314-6, Pasadena, CA 91101; gxh@ipac.caltech.edu, lee@ipac.caltech.edu, hroussel@irastro.caltech.edu, kartik@astro.caltech.edu.
[7] Department of Astronomy, Yale University, New Haven, CT 06520; murphy@astro.yale.edu.
[8] Department of Physics, Bucknell University, Lewisburg, PA 17837; mthornle@bucknell.edu.
[9] NASA Ames Research Center, MS 245-6, Moffett Field, CA 94035; hollenba@ism.arc.nasa.gov.

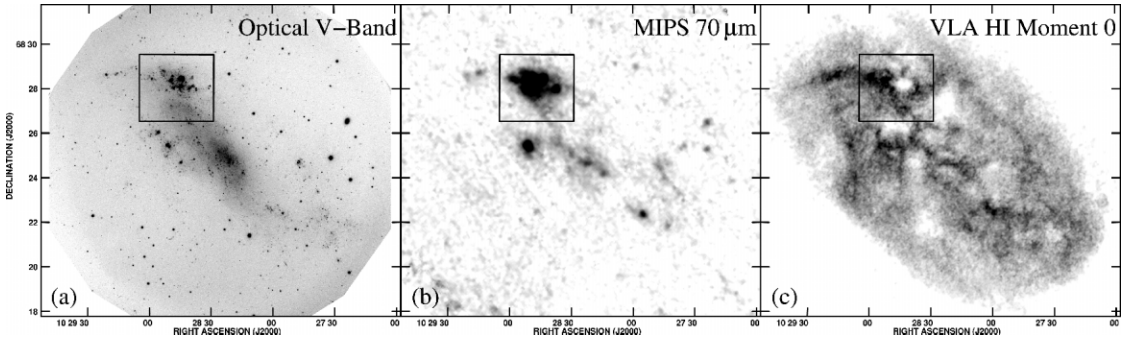

FIG. 1.—(*a*) Optical *V*-band; (*b*) MIPS 70 μm; and (*c*) H I images of IC 2574. Note that the SGS region dominates the far-IR luminosity of IC 2574, although emission is associated with other SF regions. The box in each field denotes the area shown in Fig. 2 and is ~4.4 kpc × 3.8 kpc at the adopted distance.

(2003). IC 2574 was observed for 71 minutes in Infrared Array Camera (IRAC) mosaicking mode on 2004 October 28 and 29; Multiband Imaging Photometer for *Spitzer* (MIPS) scan-mapping mode observations were obtained on 2004 November 1 and 3, for a total of 127.6 minutes. All data were processed by the SINGS pipelines. The IRAC pipeline processes basic calibrated data images; flux levels are uncertain at the ~10% level. The MIPS Instrument Team Data Analysis Tool (Gordon et al. 2005) was used to process the MIPS data. Systematic uncertainties (e.g., detector nonlinearities, time-dependent responsivity variations, background removal, etc.) limit the absolute flux calibration to ~10% at 24 μm and to ~20% at 70 and 160 μm. Fluxes were measured after convolution to the (38″ FWHM) 160 μm MIPS beam, using kernels derived from observations of a bright star (IRAC) or from STinyTim models, smoothed to match the observed point-spread functions (PSFs) (assuming a 25 K blackbody, suitable for the dust temperatures derived; MIPS).

3. MULTIWAVELENGTH EMISSION FROM THE SGS

The SGS region provides the bulk ($\simeq$50% at 24 and 70 μm) of the total infrared (TIR) luminosity of IC 2574 at wavelengths longer than ~5 μm. In Figure 1 we present a comparison of the total galaxy emission in the optical *V* band, the MIPS 70 μm band, and the H I spectral line. Note in Figure 1*c* that IC 2574 contains numerous H I shells. (Walter & Brinks [1999] identify 48 holes and shells in the ISM; the SGS studied here corresponds to No. 35 from that study.)

In Figure 2 we present images of the SGS region at nine different wavelengths. Note from the optical (*V*-band; Fig. 2*a*) and near-IR (IRAC 3.6 μm; Fig. 2*b*) images that the progenitor stellar cluster lies directly interior to the H I shell (see also Stewart & Walter 2000); this is one of the clearest examples of a kinematically distinct gaseous shell with the parent cluster still visible. By 8 μm (see Fig. 2*c*) the spectral energy distribution of the cluster has fallen below the detection limit, and emission from hot dust and gas dominates; variations in emission in the MIPS bands (Figs. 2*d*–2*f*) indicate a wide variety of dust temperatures and spectral energy distributions. Note that the shell morphology is still evident at 70 and 160 μm; the diffuse emission in the shell is most likely caused by the MIPS PSF profiles, which spread flux from high surface brightness regions onto arcminute scales (i.e., a few times the MIPS 160 μm PSF FWHM). Comparison of the MIPS, Hα, and radio continuum images (Figs. 2*g* and 2*h*) shows a wide variation in the relative ratios. Finally, the H I distribution (Fig. 2*i*) shows the H I shell very clearly; it is expanding into a nonuniform medium that may partially explain the variety of dust properties around the shell rim.

Flux densities were extracted in the apertures shown in Figure 2 (see Table 1); these regions were selected to encompass the mid-IR, far-IR, Hα, and H I emission peaks with the minimum number of apertures and amount of overlap. (Note that some apertures contain distinct emission properties at different wavelengths; e.g., SGS 1 shows a pronounced difference in Hα and radio continuum morphologies). The size of these apertures corresponds to the FWHM (38″ = 740 pc) of the MIPS 160 μm beam. Aperture correction factors have not been applied to the values shown in Table 1; the extent of the apertures for all wavelengths up to the MIPS 70 μm band (sampling more than 2, 6, 16, and 36 times the FWHM at MIPS 70 μm, MIPS 24 μm, IRAC 8 μm, and IRAC 3.6 μm, respectively) should imply relatively small aperture correction effects at these wavelengths. There will be some aperture effects at MIPS 160 μm and potentially at 70 μm as well, although the quantification of these factors depends on many parameters (including the distribution of light within the aperture, the location and brightness of neighboring sources, and many others).

4. VARYING DUST CONDITIONS IN THE SGS REGION

The characteristics of the dust change dramatically between apertures. There are appreciable variations in the dust temperature; $f_\nu(70\ \mu\text{m})/f_\nu(160\ \mu\text{m})$ varies by a factor of ~3, with the warmest dust in regions SGS 3 and SGS 5. Fitting blackbody functions modified by a λ^{-2} emissivity to the 70 and 160 μm MIPS images (see, e.g., Bianchi et al. 1999), these fluctuations correspond to a temperature range of ~23–29 K (averaged over each aperture; see Table 1). Note that the warmest dust is found in regions that have the highest Hα flux; the coolest dust is found in region SGS 2, which is at the largest distance from the SGS itself and also shows the lowest Hα flux. Interestingly, region SGS 4, which shows the highest flux density in all *Spitzer* bands, does not show the highest Hα flux.

Comparing the far-IR, Hα, and H I morphologies, it is evident that all regions except SGS 3 occupy areas with high H I surface brightness (H I column densities $\gtrsim 2 \times 10^{21}$ cm^{-2}). SGS 3 is the region with the largest Hα and 6 cm radio continuum fluxes, arguing for strong active SF, and also the highest $f_\nu(70\ \mu\text{m})/f_\nu(160\ \mu\text{m})$ dust temperature ratio. Given the age of the shell ($\simeq$15 Myr) and the expected lifetimes of H II regions and associated thermal radio continuum emission ($\lesssim$ 30 Myr), this shell may be initiating rapid SF that quickly disperses the local gas supply.

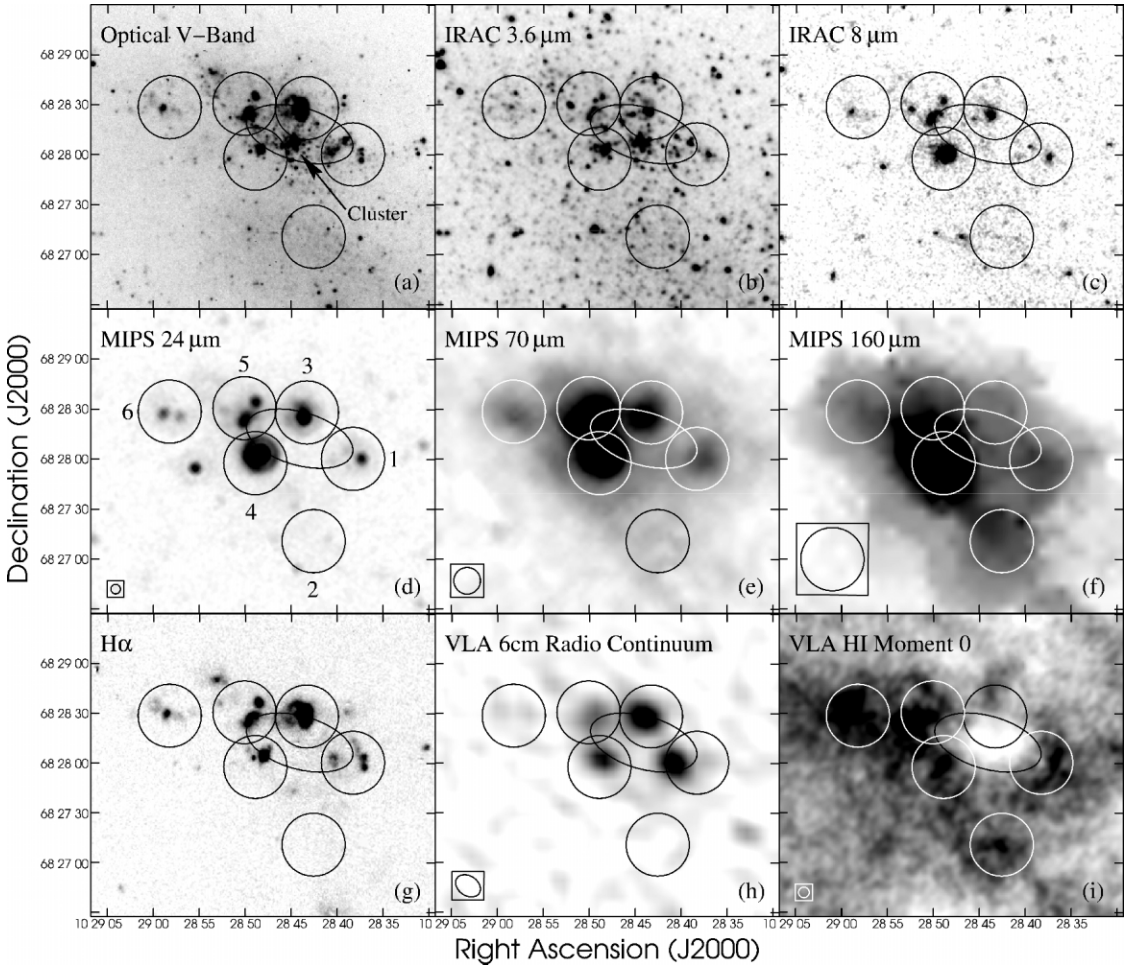

FIG. 2.—Images of the SGS region at nine different wavelengths (see Fig. 1 for location): (*a*) optical *V*-band; (*b*) and (*c*) IRAC 3.6 and 8 μm, respectively; (*d*)–(*f*) MIPS 24, 70, and 160 μm, respectively; (*g*) continuum-subtracted Hα; (*h*) 6 cm radio continuum; and (*i*) H I zeroth-moment image. The location of circular apertures SGS 1– 6 are overlaid and labeled in panel (*d*); the SGS is shown as an ellipse in each frame. In panels (*d*)–(*f*) and (*i*), the beam sizes (FWHM) are shown as boxed circles at bottom left.

4.1. *Variations in the IR vs.* Hα *Ratio*

In principle, all ultraviolet (UV) photons within dusty environments will be absorbed and reradiated in the IR; thus, there should exist a correlation between the IR luminosity and other SFR indicators, such as Hα emission. However, this simple scenario can become complicated in different environments, with dependences on stellar populations, dust content, etc. (see Kennicutt 1998 for a more detailed discussion). In the case of (typically low-metallicity) dwarf star-forming galaxies such as IC 2574, the correlation between various SFR indicators may be especially complicated, given their low dust contents and IR luminosities. Dust extinction effects (in both an absolute and differential sense) on the Hα fluxes in the SGS are minimal, based on two independent lines of evidence: first, the UV imaging study of this region by Stewart & Walter (2000) shows typical line-of-sight reddening values in the wavelength range around Hα of $A_R \simeq 0.15$ mag, with a maximum of $\sim$0.3 mag; second, new *Hubble Space Telescope* (*HST*)/Advanced Camera for Surveys (ACS) imaging and color-magnitude diagram analysis of this region (E. D. Skillman 2005, private communication) easily separates the blue helium-burning and main-sequence stars, which at this metallicity are separated by $\simeq$0.2 mag in $(V - I)$ color.

We find that the L(Hα)/L(TIR) ratio is systematically higher (by factors of $\sim$10; see Table 1) in regions that are bright in Hα compared to more quiescent regions. If one were to naively convert the Hα and IR fluxes to SFRs (using the relations of Kennicutt [1998] and Dale & Helou [2002]), the SFR(Hα) values would be systematically higher (by factors of $\sim$10) than those derived from the TIR luminosity in the active regions. Since the Kennicutt (1998) far-IR calibration assumes complete absorption of the starlight, this factor of 10 difference implies a typical Hα extinction in these regions of about 10% [A(Hα) $\sim$ 0.1 mag]. This is roughly consistent with the range of values cited above and suggests caution in the application of SFR relations based on TIR luminosities in low-metallicity environments. Note that the variations in the L(Hα)/L(TIR) ratio are not due only to varying spatial resolutions between Hα and 160 μm; we tested the severity of this effect by convolving the Hα image to the 160 μm resolution and find that the L(Hα)/L(TIR) ratio still varies by factors of $\sim$5 within the SGS region (see Table 1).

4.2. *Variations in the Radio–Far-IR Correlation*

Assuming that the TIR fluxes (derived by applying eq. [4] from Dale & Helou [2002]) and the radio continuum emission are related via a constant value [$q \propto \log (S_{\rm TIR}/S_{\rm RC})$; see, e.g., Bell (2003) for details], we derive strong variations in the value of q(TIR/radio) throughout the SGS region (see Table 1). The mean value of "q" derived within the SGS region ($\simeq$3.0) is

TABLE 1

DUST EMISSION AND DERIVED PROPERTIES IN THE IC 2574 SUPER GIANT SHELL[a]

Parameter	SGS 1	SGS 2	SGS 3	SGS 4	SGS 5	SGS 6	SGS Total
α (J2000)	10 28 38.275	10 28 42.559	10 28 43.301	10 28 48.912	10 28 50.102	10 28 58.260	10 28 44.1
δ (J2000)	68 28 00.44	68 27 10.98	68 28 28.32	68 27 57.835	68 28 30.76	68 28 28.66	68 28 12.6
Hα flux[b]	37 ± 6	7.5 ± 1.3	102 ± 20	49 ± 7	57 ± 9	17 ± 3	380 ± 60
Hα convolved flux[c]	28 ± 6	8.5 ± 1.3	66 ± 20	37 ± 7	48 ± 9	12 ± 3	380 ± 60
IRAC 3.6 μm flux density	1.4 ± 0.2	1.6 ± 0.2	1.9 ± 0.3	2.0 ± 0.3	1.8 ± 0.3	1.1 ± 0.2	28 ± 4
IRAC 4.5 μm flux density	1.3 ± 0.2	1.4 ± 0.2	1.7 ± 0.3	1.9 ± 0.3	1.7 ± 0.3	1.2 ± 0.2	29 ± 4
IRAC 8.0 μm flux density	1.1 ± 0.2	1.1 ± 0.2	1.5 ± 0.2	2.9 ± 0.4	1.9 ± 0.3	0.9 ± 0.1	22 ± 3
MIPS 24 μm flux density	5.3 ± 0.8	2.6 ± 0.4	12 ± 2	24 ± 4	15 ± 2	4.6 ± 0.7	100 ± 20
MIPS 70 μm flux density	110 ± 20	70 ± 20	160 ± 30	250 ± 50	240 ± 50	97 ± 20	1900 ± 400
MIPS 160 μm flux density	150 ± 40	160 ± 40	140 ± 40	290 ± 70	250 ± 60	160 ± 40	2600 ± 650
6 cm flux density	0.63 ± 0.07	0.046 ± 0.01	0.88 ± 0.09	0.53 ± 0.06	0.50 ± 0.06	0.13 ± 0.02	3.03 ± 0.4
F(Hα)/F(TIR)	0.044	0.011	0.090	0.024	0.033	0.021	0.026
F(Hα)/F(TIR)[c]	0.034	0.012	0.058	0.019	0.028	0.014	0.026
T_{dust} (K)	26 ± 3	23 ± 3	29 ± 3	26 ± 3	28 ± 3	25 ± 3	N/A
q (TIR/radio)[d]	2.55	3.61	2.53	3.01	2.96	3.23	3.11

NOTE.—Units of right ascension are hours, minutes, and seconds, and units of declination are degrees, arcminutes, and arcseconds.

[a] All values listed in units of millijanskys, unless otherwise noted. *Spitzer* flux densities were derived without aperture corrections, using images convolved to the MIPS 160μm resolution, with foreground stars removed in the IRAC and MIPS 24 μm bands.

[b] Derived from the work of Miller & Hodge (1994); units are 10^{-14} ergs s^{-1} cm^{-2}.

[c] Using the Hα image convolved to the MIPS 160 μm FWHM = 38″.

[d] The value of q in the radio–far-IR relation, derived using the TIR flux and the radio continuum flux at 6 cm. These calculations assume a mix of thermal and nonthermal emission (i.e., $\alpha = -0.7$, where $S_\nu \sim \nu^\alpha$) for the extrapolation from 20 to 6 cm flux densities.

consistent with, although slightly larger than, the average global values found in a sample of larger spiral galaxies in the SINGS sample (Murphy et al. 2005); we find variations of $\simeq$1 dex in the value of "q" throughout the SGS region. These strong variations may be a result of the low dust content in IC 2574 (an effect of the low metal content or of dust destruction in the extreme SGS environment).

5. CONCLUSIONS

We have presented a multiwavelength study of the SGS region in IC 2574, highlighting new *Spitzer* imaging obtained as part of SINGS. The unique multiwavelength properties demonstrate that the expanding shell is dramatically affecting its surroundings by triggering SF and by altering the dust temperature and characteristics.

The *Spitzer Space Telescope* Legacy Science Program "Spitzer Infrared Nearby Galaxies Survey" was made possible by NASA through contract 1224769 issued by the Jet Propulsion Laboratory, California Institute of Technology under NASA contract 1407. The authors thank Evan Skillman for useful discussions and the anonymous referee for comments that helped to improve the manuscript.

REFERENCES

Bell, E. F. 2003, ApJ, 586, 794
Bianchi, S., Davies, J. I., & Alton, P. B. 1999, A&A, 344, L1
Dale, D. A., & Helou, G. 2002, ApJ, 576, 159
Elmegreen, B. G., & Hunter, D. A. 2000, ApJ, 540, 814
Gordon, K. D., et al. 2005, PASP, 117, 503
Karachentsev, I. D., et al. 2002, A&A, 383, 125
Kennicutt, R. C., Jr. 1998, ARA&A, 36, 189
Kennicutt, R. C., Jr., et al. 2003, PASP, 115, 928
Kim, S., Dopita, M. A., Staveley-Smith, L., & Bessell, M. S. 1999, AJ, 118, 2797
McClure-Griffiths, N. M., Dickey, J. M., Gaensler, B. M., & Green, A. J. 2002, ApJ, 578, 176
Miller, B. W., & Hodge, P. 1994, ApJ, 427, 656
———. 1996, ApJ, 458, 467
Murphy, E. J., et al. 2005, ApJ, submitted
Sánchez-Salcedo, F. J. 2002, Rev. Mex. AA, 38, 39
Stanimirovic, S., Staveley-Smith, L., Dickey, J. M., Sault, R. J., & Snowden, S. L. 1999, MNRAS, 302, 417
Stewart, S. G., & Walter, F. 2000, AJ, 120, 1794
Tenorio-Tagle, G., & Bodenheimer, P. 1988, ARA&A, 26, 145
Walter, F. 1999, Publ. Astron. Soc. Australia, 16, 106
Walter, F., & Brinks, E. 1999, AJ, 118, 273
Walter, F., Kerp, J., Duric, N., Brinks, E., & Klein, U. 1998, ApJ, 502, L143
Wilcots, E. M., & Miller, B. W. 1998, AJ, 116, 2363